

# Homologous Pairing between Long DNA Double Helices

Alexey K. Mazur

UPR9080 CNRS, Université Paris Diderot, Sorbonne Paris Cité,  
Institut de Biologie Physico-Chimique,  
13, rue Pierre et Marie Curie, Paris, 75005, France.

Molecular recognition between two double stranded (ds) DNA with homologous sequences may not seem compatible with the B-DNA structure because the sequence information is hidden when it is used for joining the two strands. Nevertheless, it has to be invoked to account for various biological data. Using quantum chemistry, molecular mechanics, and hints from recent genetics experiments I show here that direct recognition between homologous dsDNA is possible through formation of short quadruplexes due to direct complementary hydrogen bonding of major groove surfaces in parallel alignment. The constraints imposed by the predicted structures of the recognition units determine the mechanism of complexation between long dsDNA. This mechanism and concomitant predictions agree with available experimental data and shed light upon the sequence effects and the possible involvement of topoisomerase II in the recognition.

PACS numbers: 87.15.-v, 87.15.ag, 87.15.ap, 87.14.gk

Mutual recognition between dsDNA with identical sequences is a long-standing enigma in molecular biology [1]. It is involved in processes including pre-meiotic and somatic pairing of homologous chromosomes [2, 3], repeat-induced DNA modifications [4–6] and double strand break repair [7]. Recognition is generally assumed to occur similarly to homologous recombination, i.e., due to recruited proteins that temporarily open dsDNA and make possible the cross-stranded Watson-Crick (WC) base pairing. However, this would require proteins with very special functions, whereas so far searches including genome-wide genetic screens [8–10] have not revealed suitable candidates. Direct DNA-DNA recognition has been suggested as an alternative solution [1, 11–13]. Two possible mechanisms have been considered in the recent years: (1) Attractive long-range electrostatic interactions between B-DNA with identical sequence-dependent conformations [14, 15] and (2) a strand exchange between two dsDNA to form the PX-DNA motif used in DNA-origami nanotechnology [16, 17]. These models explained available biological data and fit well with the results of *in vitro* experiments in cell-free conditions [18, 19]. However, they cannot account for the phenomenon of recognition between partial homologies recently discovered by Gladyshev and Kleckner [20]. These authors studied the sequence dependence of repeat-induced point mutations (RIPs). RIPs occur in fungi cells that somehow identify and target for mutation any long repeated sequence in genome [4, 5]. Strikingly, the recognition occurs with even 25% homology, provided that it is distributed in a series of triplets spaced by 11 or 12 base pair steps (bps) [20]. Two dsDNA with such sequences cannot form PX-DNA [21] and neither they can be structurally similar, therefore, the RIP data [20] do not fit with the mechanisms of direct recognition [14–17]. These new observations are also difficult to reconcile with any recognition via WC pairing. Indeed, the RIP data indicate that the

two dsDNA remain torsionally rigid and the recognition improves with the number of active triplet frames rather than the integral homology [20]. In contrast, local melting should zero the twisting rigidity, and hybridization of continuous homologous ssDNA should be orders of magnitude more efficient than pairing of the same number of base pairs in periodically spaced triplets.

In the present study I analyze the possibility of dsDNA recognition through direct binding by major grooves. It has been noticed long ago that the major groove edges of WC base pairs have complementary hydrogen bonding (H-bonding) patterns [22, 23]. An infinite helical quadruplex using major groove association between WC pairs was predicted by manual modeling [11] and discussed as an intermediate state in homologous recombination [12, 24]. Experimentally, such structures were not found, but the possibility of major groove H-bonding was confirmed [25, 26]. Using methods of quantum chemistry (QC), molecular mechanics (MM), and molecular dynamics (MD), I show that direct dsDNA binding by complementary major grooves should be considered as a probable pathway for direct homology recognition. The admissible recognition conformations are dictated by structural constraints and they explain experimental data better than alternative mechanisms.

Fig. 1 illustrates the hypothetical association of two identical B-DNA structures by merging the major grooves. The quadruplex in the right panel has four grooves, namely, two minor grooves of the constituting double helices and two new grooves, hereafter called secondary, formed between the two juxtaposed major grooves. The interior of this structure consists of parallel base tetrads shown in Fig. 2. They are formed by identical WC pairs linked by two new H-bonds also called secondary. Such tetrads were experimentally confirmed for both types of WC pairs using short ssDNA hairpins [25, 26]. Fig. 2 and Table I reveal that the

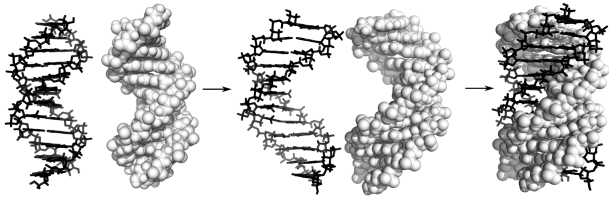


FIG. 1: Helical quadruplex formed from two WC double helices. On the left, two canonical B-DNA duplexes are shown facing one another by their major grooves. The middle panel displays their conformations in the complexed state. They are slightly stretched and untwisted to a helical pitch about 12.9. The right panel shows a right-handed quadruplex formed by major groove association.

secondary H-bonds are shorter and stronger than their sisters in WC pairs. These results were obtained by QM optimizations of tetrad geometries in vacuum [27]. Earlier studies of WC base pairs indicate that such calculations reproduce experimental trends, with the energy differences scaled down due to the polar environment [28]. The stabilization energy of the GC/GC tetrad is surprisingly large, namely, the energy of two H-bonds appears similar to that of the WC pair with three H-bonds. This non-pair-additive electrostatic effect is due to the large dipole moment and high polarizability of the GC pair [27]. Because of this non-pair-additivity, molecular mechanics significantly underestimates the strength of secondary H-bonding, which is important for interpretation of other results.

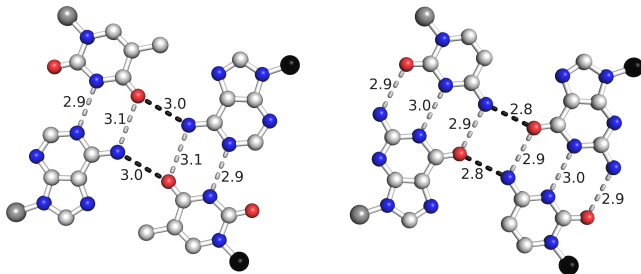


FIG. 2: (Color online) Mutual recognition between identical WC base pairs via major-groove edges. Large spheres of two different colors correspond to C1' atoms of different dsDNA. Geometry and stabilization energies (Table I) of individual base pairs and tetrads were evaluated by vacuum geometry optimizations at MP2/6-311G(d) level of theory [27]. The computed H-bond lengths are shown in angstroms (Å). The secondary H-bonds are distinguished by darker dashed lines.

The B-DNA conformations in the left panel of Fig. 1 look predisposed for association because they resemble separated fibers of a two-strand twine. In the complex, the double helices are spun so that quadruplexes longer than one turn cannot fall apart even in the absence of the secondary H-bonding. The complex is easily built by

TABLE I: Vacuum stabilization energies,  $U$  (kcal/mol), computed by QC and MM methods as described elsewhere [27]. The energy of WC pairing was estimated as the difference between the vacuum energy of the pair and that of constituting nucleobases. For secondary pairing the energy is obtained as the difference between the tetrad energy and that of constituting base pairs. The WC pairs are denoted by the standard two-letter code. Slashes denote the secondary pairing. The  $U_{\text{MM}}$  values were computed with the AMBER forcefield [29]. For WC pairs these results agree with earlier data [28].

Energy	GC	GC/GC	AT	AT/AT
$U_{\text{QC}}$	29.5	26.4	16.2	12.6
$U_{\text{MM}}$	28.3	19.5	12.9	10.6

making a cylinder from stacked tetrads and then properly placing backbone strands at its surface [11], but it cannot be obtained by docking two dsDNA following the arrows in Fig. 1. To this end, the two initial structures must be untwisted to an almost flat ladder, joined, and then relaxed. Even small untwisting of dsDNA leads to dissociation of the two strands [30], therefore, this simple pathway is not feasible. The question is if there exists an alternative pathway that can join the left and right hand states in Fig. 1. To get an idea of the transition state of such a pathway, preliminary all-atom MD simulations were run with quadruplexes of different lengths and sequences with explicit ions and water [27]. In the course of these tests, it became clear that a required transition state can be obtained by separating 5 bps at both ends of the quadruplex, which gives four B-DNA "paws" protruding from the core, and then keeping the paws wide open for the time necessary to relax the helical twist to that of B-DNA.

The idea of the following MD simulations is similar to some early MD studies [31] and it is explained in Fig. 3. In all subsequent modeling only GC-alternating sequences were used. We start from a predicted barrier state and try to reach both quadruplex and unbound states in free dynamics, without any guiding restraints. If we are lucky the trajectories in both directions would go downhill on the energy landscape. Even in this case, however, a straightforward simulation requires enormous time resources. Therefore, to obviate entropic barriers, a Maxwell demon approach is applied. A bundle of trajectories is started from the same state with different random velocities. All trajectories are followed visually and stopped after a certain time interval (usually about 2 ns) or when an interesting local transition towards dissociation/binding occurred somewhere within the bundle. One of the final states considered as most advanced towards dissociation/folding is selected and used as the start of a new bundle of trajectories. After several iterations in the two opposite directions one gets two trajectories leading to unbound and quadruplex states, respectively. The trajectories are continuous in the coordinate

space, with velocities periodically randomized. By inverting one of them we obtain a pathway between the terminal states in Fig. 1 that involves only elastic deformations and does not require base pair opening.

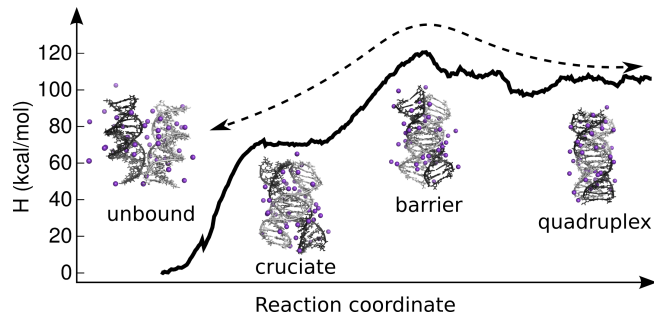


FIG. 3: The overall plan of MD simulations and the approximate energy profile along the transition pathway. Trajectories started from a predicted barrier structure and continued in the two opposite directions. The reaction coordinate was constructed as explained in the text, with the energy profile smoothed by averaging with a sliding window of about 2 ns.

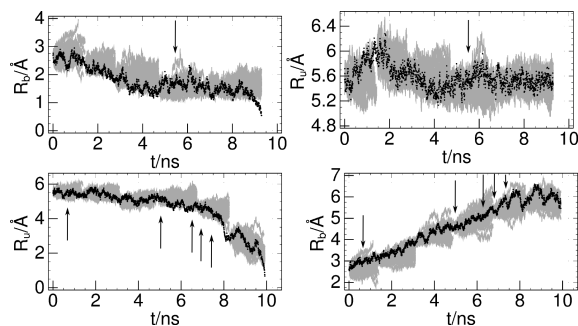


FIG. 4: Time traces of root mean square deviations (RMSD). The RMSDs from bound (quadruplex) ( $R_b$ ) and unbound ( $R_u$ ) states (see Fig. 3) were computed for two double helices separately and averaged. The upper and lower panels display results for binding and dissociation, respectively. The gray bands are formed by traces of bundles of 32 trajectories computed as explained in the text. The restart points can be distinguished by narrowings of these bands. The black traces correspond to trajectories selected for continuation. The vertical arrows mark formation and splitting of tetrads during folding and dissociation, respectively.

The time course of the production run is illustrated in Fig. 4. A more detailed picture is provided as animation files [27]. Surprisingly, just 10 ns were necessary to reach both quadruplex and unbound states. During binding, only one complete additional tetrad was formed. A few ions and water molecules were sequestered between bases, which strongly complicated formation of secondary H-bonds. However, both secondary grooves, with characteristic chains of potassium ions between phosphates, were already formed. During dissociation the order of events was inverted, that is, the dissociation of tetrads preceded that of ions and groove opening. The starting

intermediate was probably shifted towards the quadruplex state. None of the trajectories of the first bundle displayed strong trends towards dissociation even though in two cases one boundary tetrad was split. The first of these trajectories selected for continuation towards the unbound state was not successful. The second choice worked; however, even in the fourth bundle there were trajectories that turned back to folding (see Fig. 4). The dissociation accelerated after the split of three tetrads.

The energy profile shown in Fig. 3 was evaluated as follows. New trajectories were re-started similarly to the main run from 280 states equally spaced in time along the transition pathway, and the average total energy was evaluated for 0.5 ns after short equilibration. This profile is approximate and lacks the entropic contribution of the free energy, but it gives an estimate of shape and the order of magnitude of the values involved. Thorough calculations using umbrella sampling and the weighted histogram analysis would be prohibitively costly, and they usually give qualitatively similar profiles scaled down by one-two orders of magnitude [32]. The apparently large energies obtained are not prohibitive. First, all available data indicate that the recognition requires long incubation stages from hours to weeks, therefore, the corresponding free energy barrier can well reach 10-20 kcal/mol. Second, the plateau at 70 kcal/mole mainly depends upon the type and concentration of ions. The neutralizing amount of monovalent ions used here was not meant to reproduce real conditions that probably involve a combination of mono and divalent ions with higher concentrations. Finally, the energy values in Fig. 3 would be much larger for alternative recognition models that include strand dissociation.

The plateau at 70 kcal/mole in Fig. 3 indicates that structures with 3-4 stacked tetrads can represent a metastable state with a local free energy minimum. In short quadruplexes the tetrads are propeller twisted and slightly non-parallel, which allows the paws protruding from the core to be separated without strong bends. With the length of the tetrad stack increased, the tetrads become more parallel and stronger bending in the paws is required. This explains the emergence of the plateau in Fig. 3 that can well transform into an energy minimum with stronger secondary H-bonds corresponding to Table I. I suggest that, under appropriate ionic conditions, the free energy in this minimum is lower than that of the unbound state. In contrast, the additional bending strain responsible for the central energy barrier cannot be eliminated. With increased DNA length this barrier would broaden and eventually become a plateau. Under these assumptions, the cruciate structures with short quadruplexes of 3-4 stacked tetrads work as recognition units in homologous alignment of long double helices.

Conformations of the cruciate units observed in dynamics were used for predicting the complexes of long DNA (Fig. 5). They were built in several steps by com-

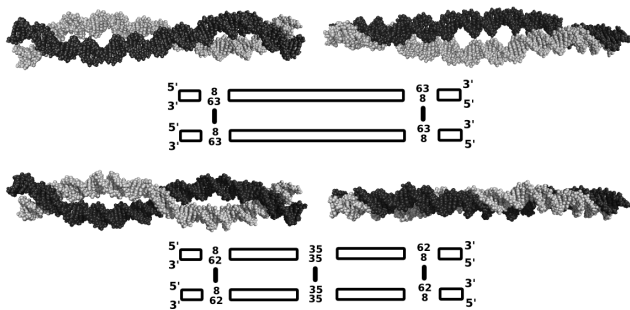


FIG. 5: Modeled complexes of long dsDNA obtained as explained in the text. The upper and lower panels demonstrate paranemic and plectonemic modes of binding, respectively. The two columns show two perpendicular views of each structure. In the schematics below the structures, dsDNA stretches are shown as rectangles interrupted by recognition units. For each unit the four bases of the central tetrad are indicated, with the secondary H-bonding marked by thick vertical lines.

binning all-atom and coarse grained modeling [27]. The cruciate shape of the recognition unit and the bending rigidity of the double helix impose significant limitations upon the minimal axial separation between the pairing contacts. In the upper panels of Fig. 5 the two recognition units are separated by five helical turns. This number is identical in the two chains, therefore, the units share the same plane. For smooth connection the intermediate helices take a particular sinuous shape. The high bending rigidity of DNA straightens these helices and pushes them close to each other against repulsive electrostatic forces. The helix-helix orientations are not optimal according to earlier predictions and simulations [33, 34] and the corresponding energy contributes to the high energy barrier of binding. Even though the bend angles in the helical stretches are admissible, they are strained because all local bends must have concerted values and directions. With the growing distance between the recognition units, this strain is relieved and its energy can be compensated by that of binding. For complete homologies, the experimental recognition threshold of 200-300 bp probably corresponds to a relatively small number of specific contacts, which explains the drastic disappearance of recognition at these DNA lengths.

The upper and lower structures in Fig. 5, respectively, demonstrate paranemic and plectonemic contacts between two dsDNA. In the latter case the linear density of recognition units is two times higher. Plectonemes like that in Fig. 5 are possible when the two terminal recognition units are separated by an odd number of helical turns. In this case the middle unit is rotated by  $180^\circ$  and shifted by a half-integer number of turns. In a similar plectoneme with an even number of helical turns the central segments of the two double helices would face one another by their minor grooves. In this case, one can consider the possibility of a cruciate recog-

nition unit formed by the hypothetical strand exchange mechanism [12]. The paranemic contacts can be always formed by loops protruding from chromosomes. In contrast, plectonemic contacts require the topoisomerase II (Top2) activity because otherwise every right-hand turn with three recognition units must be compensated by a left-hand turn, with no recognition units and a very high entropic penalty. Interestingly, the loss or inhibition of Top2 was shown to partially compromise the pairing of homologous chromosomes in cell cultures [3]. It would be interesting to check if this effect also plays a role in RIP.

Recognition via discrete units spaced by several helical turns represents an extension of one of the models considered by Gladyshev and Kleckner [20] and it sheds new light upon their data. Notably, the helical pitch of the quadruplex structure in Fig. 1 (12.9) is larger than that of B-DNA (10.5). Therefore, the average helical pitch in complexes shown in Fig. 5 grows with the density of recognition units, which explains the higher RIP efficiency for sequences with periods 11 and 12 bp compared to 10 bp. The large distance between the recognition units makes the constraint upon the concerted twisting in the two double helices more stringent because the amplitude of thermal torsional fluctuations grows only as a square root of the chain length. Under normal temperature, the difference between 10 and 11-bp periodicities can be compensated by thermal fluctuations for one helical turn, but not for five helical turns. In the latter case it corresponds to rotation by  $180^\circ$ . This explains strong differences in RIP activities for the some periodicities that differ by only one bp. Finally, the sequence dependence of the secondary H-bonding predicted by Table I might account for the examples of strongly different RIP for homologies that differ only by the sequence [20].

Encounters between identical DNA sequences are rare in nature, but they should be very frequent *in vitro*, therefore, one may ask why complexes shown in Fig. 5 remain almost unnoticed in chemical laboratories. In fact, they are perhaps long known, but discarded. DNA is never stored during hours and weeks in ionic solutions because it is known to slowly aggregate and deteriorate. Rare attempts to systematically study the slow evolution of DNA samples in laboratory conditions gave very perplexing results [35]. The sequence-specific association is driven by ions, with both mono and divalent cations probably involved. The binding shown in Fig. 5 occurs due to reversible interactions that are likely to be destroyed during dilution or penetration through gels. At the same time, small ion excess may lead to almost irreversible non-specific complexation. These issues are not easy to sort out and they require further experimental investigation.

In summary, the mutual recognition between two homologous B-DNA might occur due to direct complementary H-bonding of major groove surfaces in parallel alignment. The pairing of two dsDNA results in formation

of a planar cross-shaped recognition unit, with a central quadruplex of 3-4 bps and four B-DNA paws protruding in opposite directions. In a complex of two dsDNA the recognition units have to be spaced by at least several helical turns, therefore, the binding requires long double helices, but only partial homology. The recognition units are separated from the unbound state by a high energy barrier and they are stabilized by specific H-bonding as well as ion-DNA interactions. Therefore, the binding takes very long time and is very sensitive to ionic conditions. The proposed mechanism and concomitant predictions agree with earlier data and shed light upon the recent intriguing experimental results [20].

The computational resources used in this study were supported by the Initiative d'Excellence program from the French State Grant No. ANR-11-LABX-0011-01 (DYNAMO).

- 
- [1] N. Kleckner and B. M. Weiner, *Cold Spring Harb. Symp. Quant. Biol.* **58**, 553 (1993).
- [2] B. D. McKee, *Biochim. Biophys. Acta.* **1677**, 165 (2004).
- [3] B. R. Williams, J. R. Bateman, N. D. Novikov, and C. T. Wu, *Genetics* **177**, 31 (2007).
- [4] A. T. Hagemann and E. U. Selker, *Cold Spring Harbor Monograph Archive* **32**, 586 (1996).
- [5] E. U. Selker, *Adv. Genet.* **46**, 439 (2002).
- [6] J. L. Rossignol and G. Faugeron, *Experientia* **50**, 307 (1994).
- [7] A. Barzel and M. Kupiec, *Nat. Rev. Genet.* **9**, 27 (2008).
- [8] J. R. Bateman and C. T. Wu, *Genetics* **180**, 1329 (2008).
- [9] J. P. Blumenstiel, R. Fu, W. E. Theurkauf, and R. S. Hawley, *Genetics* **180**, 1355 (2008).
- [10] E. F. Joyce, B. R. Williams, T. Xie, and C. T. Wu, *Plos Genet.* **8**, e1002667 (2012).
- [11] S. McGavin, *J. Mol. Biol.* **55**, 293 (1971).
- [12] J. H. Wilson, *Proc. Natl. Acad. Sci. U. S. A.* **76**, 3641 (1979).
- [13] D. Zickler and N. Kleckner, *Cold Spring Harb. Perspect. Biol.* **7**, a016626 (2015).
- [14] A. A. Kornyshev and S. Leikin, *Phys. Rev. Lett.* **86**, 3666 (2001).
- [15] A. A. Kornyshev, *Phys. Chem. Chem. Phys.* **12**, 12352 (2010).
- [16] N. C. Seeman, *Nano Lett.* **1**, 22 (2001).
- [17] X. Wang, X. Zhang, C. Mao, and N. C. Seeman, *Proc. Natl. Acad. Sci. U. S. A.* **107**, 12547 (2010).
- [18] G. S. Baldwin, N. J. Brooks, R. E. Robson, A. Wynveen, A. Goldar, S. Leikin, J. M. Seddon, and A. A. Kornyshev, *J. Phys. Chem. B.* **112**, 1060 (2008).
- [19] C. Danilowicz, C. H. Lee, K. Kim, K. Hatch, V. W. Coljee, N. Kleckner, and M. Prentiss, *Proc. Natl. Acad. Sci. U. S. A.* **106**, 19824 (2009).
- [20] E. Gladyshev and N. Kleckner, *Nat. Commun.* **5**, 3509 (2014).
- [21] Z. Shen, H. Yan, T. Wang, and N. C. Seeman, *J. Am. Chem. Soc.* **126**, 1666 (2004).
- [22] P. O. Löwdin, in *Electronic Aspects of Biochemistry*, edited by B. Pullman (Academic Press, New York, 1964), pp. 167–201.
- [23] H. E. Kubitschek and T. R. Henderson, *Proc. Natl. Acad. Sci. U. S. A.* **55**, 512 (1966).
- [24] A. Lebrun and R. Lavery, *J. Biomol. Struct. Dyn.* **13**, 459 (1995).
- [25] A. Kettani, R. A. Kumar, and D. J. Patel, *J. Mol. Biol.* **254**, 638 (1995).
- [26] N. Zhang, A. Gorin, A. Majumdar, A. Kettani, N. Chernichenko, E. Skripkin, and D. J. Patel, *J. Mol. Biol.* **312**, 1073 (2001).
- [27] See Supplemental Material at [URL will be inserted by publisher], which includes Refs. [36–54], for additional details, comments, protocols of computations, and trajectory movies.
- [28] J. Sponer, P. Jurecka, and P. Hobza, *J. Am. Chem. Soc.* **126**, 10142 (2004).
- [29] W. D. Cornell, P. Cieplak, C. I. Bayly, I. R. Gould, K. M. Merz, D. M. Ferguson, D. C. Spellmeyer, T. Fox, J. W. Caldwell, and P. A. Kollman, *J. Am. Chem. Soc.* **117**, 5179 (1995).
- [30] Z. Bryant, M. D. Stone, J. Gore, S. B. Smith, N. R. Cozzarelli, and C. Bustamante, *Nature* **424**, 338 (2003).
- [31] S. C. Harvey and H. A. Gabb, *Biopolymers* **33**, 1167 (1993).
- [32] L. V. Bock, C. Blau, G. F. Schroder, I. I. Davydov, N. Fischer, H. Stark, M. V. Rodnina, A. C. Vaiana, and H. Grubmuller, *Nat. Struct. Mol. Biol.* **20**, 1390 (2013).
- [33] P. Varnai and Y. Timsit, *Nucl. Acids Res.* **38**, 4163 (2010).
- [34] R. Cortini, A. A. Kornyshev, D. J. Lee, and S. Leikin, *Biophys. J.* **101**, 875 (2011).
- [35] G. P. Brewwood, J. J. Deltow, and J. M. Schurr, *Biochemistry* **49**, 3367 (2010).
- [36] A. R. Srinivasan, R. R. Sauers, M. O. Fenley, A. H. Boschitsch, A. Matsumoto, A. V. Colasanti, and W. K. Olson, *Biophys. Rev.* **1**, 13 (2009).
- [37] A. A. Granovsky, firefly version 8.1.0, [www http://classic.chem.msu.su/gran/firefly](http://classic.chem.msu.su/gran/firefly).
- [38] M. W. Schmidt, K. K. Baldrige, J. A. Boatz, S. T. Elbert, M. S. Gordon, J. J. Jensen, S. Koseki, N. Matsunaga, K. A. Nguyen, S. Su, et al., *J. Comput. Chem.* **14**, 1347 (1993).
- [39] I. S. Joung and T. E. 3rd Cheatham, *J. Phys. Chem. B.* **112**, 9020 (2008).
- [40] J. Wang, P. Cieplak, and P. A. Kollman, *J. Comput. Chem.* **21**, 1049 (2000).
- [41] A. Perez, I. Marchan, D. Svozil, J. Sponer, T. E. Cheatham, C. A. Lughton, and M. Orozco, *Biophys. J.* **92**, 3817 (2007).
- [42] M. Zgarbova, F. J. Luque, J. Sponer, T. E. Cheatham, M. Otyepka, and P. Jurecka, *J. Chem. Theory Comput.* **9**, 2339 (2013).
- [43] H. J. C. Berendsen, J. R. Grigera, and T. P. Straatsma, *J. Phys. Chem.* **91**, 6269 (1987).
- [44] U. Essmann, L. Perera, M. L. Berkowitz, T. Darden, H. Lee, and L. G. Pedersen, *J. Chem. Phys.* **103**, 8577 (1995).
- [45] H. J. C. Berendsen, J. P. M. Postma, W. F. van Gunsteren, A. DiNola, and J. R. Haak, *J. Chem. Phys.* **81**, 3684 (1984).
- [46] A. K. Mazur, *J. Comput. Chem.* **18**, 1354 (1997).
- [47] A. K. Mazur, *J. Chem. Phys.* **111**, 1407 (1999).
- [48] A. K. Mazur, *J. Am. Chem. Soc.* **120**, 10928 (1998).
- [49] A. K. Mazur, *J. Phys. Chem. B* **102**, 473 (1998).

- [50] A. K. Mazur, *Biophys. J.* **91**, 4507 (2006).
- [51] A. K. Mazur, *Phys. Rev. Lett.* **105**, 018102 (2010).
- [52] A. K. Mazur, *Phys. Rev. E* **84**, 021903 (2011).
- [53] W. K. Olson, M. Bansal, S. K. Burley, R. E. Dickerson, M. Gerstein, S. C. Harvey, U. Heinemann, X.-J. Lu, S. Neidle, Z. Shakked, et al., *J. Mol. Biol.* **313**, 229 (2001).
- [54] A. K. Mazur, *J. Phys. Chem. B* **113**, 2077 (2009).

## SUPPLEMENTAL MATERIAL

### Quantum chemistry and molecular mechanics calculations

The chemical geometry and stabilization energies of WC pairs and tetrads corresponding to major groove binding of two B-DNA were evaluated by vacuum geometry optimizations at MP2/6-311G(d) level of theory. This accuracy is similar to that in earlier studies for nucleobases and base pairs [28, 36]. The Firefly QC package [37] was used, which is partially based on the GAMESS (US) [38] source code. For comparison, similar energy minimizations were carried out using standard MM approximations with the all-atom AMBER forcefield [29]. AMBER is known to reasonably reproduce the quantum energies of WC base pairing in vacuum [28]. To my knowledge, for the secondary H-bonds this was never checked.

The comparison makes sense and is necessary only for nearly planar configurations because, in dsDNA complexes of interest, non-planar configurations are sterically impossible. In vacuum, however, unconstrained energy minimizations starting from planar configurations for tetrads in Fig.1 usually result in buckling because the out-of-plane deformations are virtually free, whereas non-planar configurations have lower energies due to additional atom-atom contacts. Moreover, MP2-minimizations of guanine and cytosine give non-planar pyramidal conformations of the exocyclic amino groups, which is not reproduced in MM. For consistent comparison, therefore, the energy minimizations were carried out with the overall planarity imposed by constraints. To this end, the structures of bases were described using natural internal coordinates, that is, bond lengths, bond angles and dihedrals. Bases in WC pairs and tetrads were linked by virtual bonds. The relative orientation of two linked bases is described by six internal coordinates corresponding to virtual bonds and angles formed at the junction. The set of six junction coordinates involves one distance, two planar angles, and three dihedrals. The overall planarity is imposed by freezing the dihedrals. The junctions were chosen so that the free planar angles could not come close to zero or  $\pi$  during minimizations. In total, nine junction dihedrals were frozen to impose the planarity of tetrads. In these conditions, the exocyclic amino groups appeared to remain planar without additional constraints. The constrained minimizations were carried out using the built-in options of the Firefly QC package [37]. The results are shown in Table I.

For WC pairs, both the QC and MM energies in Table S1 are close to those reported earlier [28], which means that these values are not very sensitive to the planarity constraints and other methodological differences from earlier studies. The dipole moments also included in Table S1 are important because dipole-dipole interactions

TABLE S1: Computed stabilization energies,  $U$  (kcal/mol), and dipole moments,  $D$  (debye), of planar nucleobase complexes. The energy of WC pairing was estimated as the difference between the vacuum energy of the pair and that of constituting isolated nucleobases, respectively. For secondary pairing the energy is obtained as the difference between the tetrad energy and that of constituting base pairs, respectively. The WC pairs are denoted by the standard two-letter code. Slashes denote the secondary pairing.

Complex	$U_{QC}$	$D$	$U_{MM}$
A	-	2.55	-
T	-	4.03	-
AT	16.2	1.27	12.9
AT/AT	12.6	0.00	10.6
G	-	6.61	-
C	-	6.27	-
GC	29.5	6.09	28.3
GC/GC	26.4	0.00	19.5

often give significant electrostatic contributions to the stabilization energies. Notably, the dipole moment of the AT pair is significantly smaller than those of adenine and thymine bases, indicating that the corresponding vectors in the pair are antiparallel, which increases the energy of pairing. This interaction can involve a significant non-pair-additive component because antiparallel molecular dipoles induce additional electron polarization that enhances the electrostatic attraction. This explains the significantly larger quantum stabilization energy of the AT pair compared to MM (Table S1). In contrast, the large dipole moments of guanine and thymine in the GC pair are strongly non-collinear, which explains the much better agreement between the QC and MM stabilization energies.

Based upon the foregoing considerations one can anticipate a significant contribution to the stabilization energy of tetrads from the dipole-dipole polarization of constituting WC pairs. Indeed, the tetrad dipole moment is zero by symmetry, that is, the dipole moments of the constituting pairs are exactly antiparallel. The results shown in Table S1 confirm this prediction. For the AT/AT tetrad the QC and MM stabilization energies are relatively close because the dipole moment of the AT pair is small. In contrast, the quantum stabilization energy of the GC/GC tetrad is strikingly large. Two secondary H-bonds formed in the GC/GC tetrad give the stabilization energy similar to that due to three H-bonds of the GC pair.

The stabilization energy of the AT/AT tetrad is somewhat smaller than that of the AT pair, with a somewhat larger difference for  $U_{QC}$  than for  $U_{MM}$ . A part of this difference is due to two steric clashes between the thymine methyls and N7 atoms of adenines in the AT/AT tetrad (see Fig. 1). In the strictly planar configuration, these contacts hinder formation of optimal geometry of

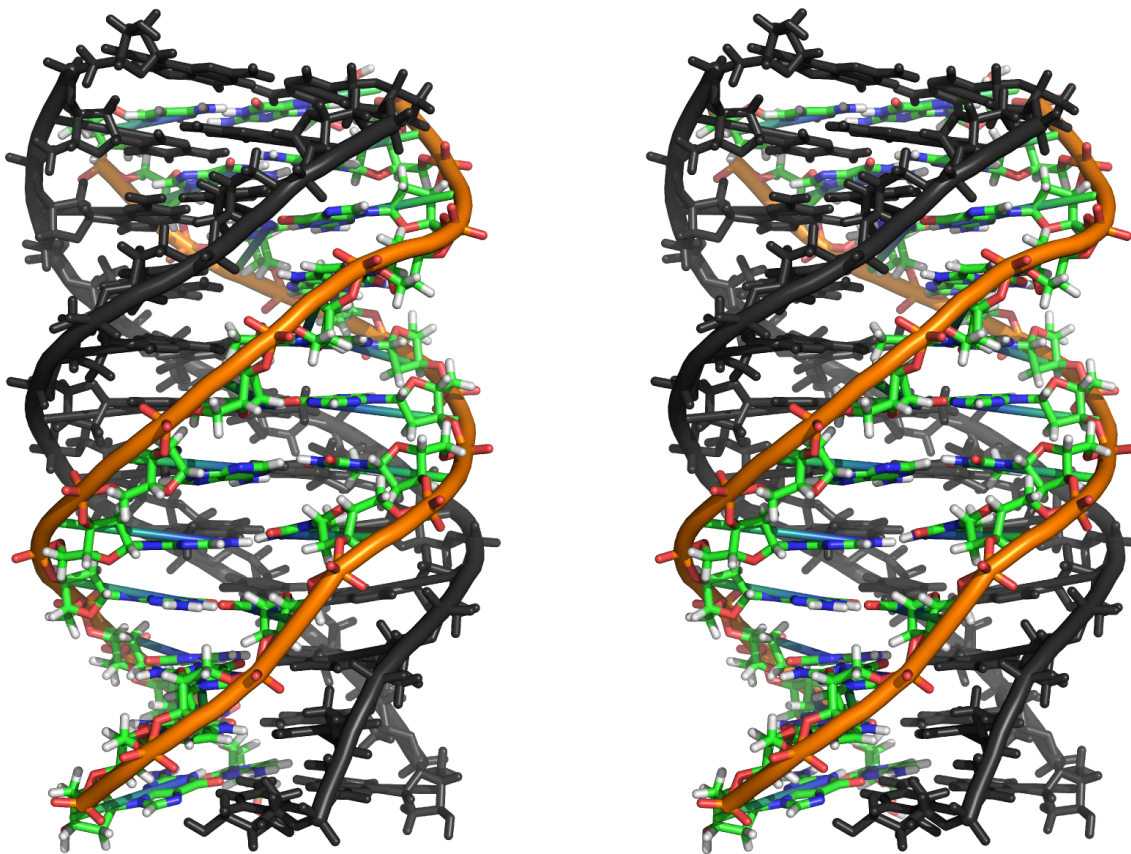


FIG. S1: A snapshot from an MD trajectory of a quadruplex formed by two dodecamer double helices with the self-complementary sequence CGCGAATTCGCG. One of the helices is colored black for distinction. A cross-eyed stereo image is shown.

secondary H-bonds. When the energy minimization is continued without the planarity constraints these clashes are readily relieved by small propeller twisting, with the overall planarity perturbed insignificantly. The corresponding energy gain is about 2 kcal/mole. Further minimization leads to buckling of the tetrad and large-scale rotation of base pairs toward a stacked configuration, which occurs with very slow fall of energy. Qualitatively similar results were obtained for GC/GC tetrads with 5-methylcytosines (not shown). These computational observations suggest that 5-methylation of pyrimidine bases does not cause steric problems for homologous pairing between dsDNA although further studies are required to take into account the solvent and structural environment.

#### Molecular dynamics simulations

DNA duplexes of different lengths and sequences were modeled in aqueous environment neutralized by potassium ions [39], using a recent version of the all-atom AMBER forcefield [29, 40–42] with SPC/E water [43] in periodic boundaries. The electrostatic interactions were treated by the SPME method [44], with the common val-

ues of Ewald parameters, that is 9 Å truncation for the real space sum and  $\beta \approx 0.35$ . The temperature was maintained by the Berendsen algorithm [45] applied separately to solute and solvent with a relaxation time of 10 ps. To increase the time step, MD simulations were carried out by the internal coordinate method (ICMD) [46, 47], with the internal DNA mobility limited to essential degrees of freedom. The rotation of water molecules and internal DNA groups including only hydrogen atoms was slowed down by weighting of the corresponding inertia tensors [48, 49]. The double-helical DNA was modeled with free backbone torsions as well as bond angles in sugar rings, but rigid bases and phosphate groups. The net effect of these constraints upon DNA dynamics is not significant, which was checked earlier through comparisons with conventional Cartesian MD [48, 50]. The time step was 0.01 ps.

Helical quadruplex conformations were constructed in several steps using in-house software. Ideal quadruple helices were built from dsDNA with homopolymer polyG-polyC sequences. To this end, two dsDNA trimers were docked manually in vacuum and the structure was energy minimized in internal coordinates with constraints ensuring that in each single strand homologous internal



coordinates at different steps had identical values. The resulting structure was elongated by adding tetrads one by one, with energy minimizations repeated from conformations obtained in the previous step. The helical backbone conformations obtained were used for building quadruplexes with other sequences. The subsequent MD simulations were carried out using standard equilibration and production protocols earlier applied to dsDNA [51, 52].

A few preliminary MD simulations involved helical quadruplexes formed by double helical polyG-polyC decamers, polyGC pentadecamers and dodecamers with the self-complementary sequence CGCGAATTCGCG. A snapshot from the last trajectory is shown in Fig. S1. The following qualitative computational observations seemed most interesting for the present study. Originally [11], the quadruplex structure formed by merging two dsDNA seemed appealing because of (i) the compactness and (ii) the complementarity of the H-bonding. Both these features turned out to be inessential. In fact, the secondary grooves remain hydrated and allow water and ions to penetrate inside and even break the secondary H-bonds. This, however, is not critical for stability because the secondary grooves are sealed by a layer of ions sandwiched between the backbone phosphate groups. In one test all the secondary HB in the CGCGAATTCGCG quadruplex were canceled by adding appropriate repulsive forces, and this had virtually no effect upon the stability in the nanosecond time range. When the duplexes in the pentadecamer quadruplex are separated near one end by properly applying perpendicular stretching forces the secondary grooves are quickly closed once the stretching is switched off, but the specific H-bonding usually is not recovered completely.

According to Table S1 the AMBER forcefield significantly underestimates the relative strength of the secondary H-bonding, which certainly affected the above results. At the same time, the adsorption of cations in the secondary grooves, evident in MD, is quite probable and it can result in a strong electrostatic stabilization depending upon ion types and concentrations. In the course of these tests, it became clear that the transition state between the bound and dissociated states of two dsDNA can be obtained by separating 5 bps at both ends of the quadruplex, which gives four "paws" protruding from the core, and then keeping the paws wide open for the time necessary to relax the helical twist to that of B-DNA. The preparation of such intermediate turned out to be quite laborious because it could not be achieved by vacuum modeling. Eventually, this was done by running MD simulations of two pentadecamer dsDNA with GC-alternating sequences under visual control with restraining potentials as well as non-conservative forces adjusted *ad hoc* so that the structure was slowly pushed towards the predicted state. The resulting structure included a quadruplex core of five stacked tetrads in the middle and

four B-DNA paws of the same length protruding in different directions. The WC pairing within the duplexes was intact. The base stacking was not strictly parallel, but there was no significant deformations accompanied by water entering between bases. The duplexes were hydrated and made no direct contacts except the secondary H-bonds. All backbone torsion angles had values within the canonical B-DNA intervals. These computations involved many tens of nanoseconds of MD, which also served for slow ion diffusion and equilibration of the environment. Therefore, the subsequent production MD simulations could be started after randomization of velocities followed by short re-equilibration during a few tens of picoseconds.

### Complexes of long DNA

The structures of complexes of long DNA shown in Fig. 5 were built in several steps by combining all-atom and coarse grained modeling. The pentadecamer cruciate structures with three central tetrads and the B-DNA paws that could be continued without strong bends were selected from MD trajectories by visual inspection (see Fig. S2). In the subsequent modeling these structures remained rigid. Using the standard local base pair frames [53] the discrete wormlike rod (WLR) versions [54] of these conformations were built. The objective of the coarse-grained step was limited to construction of chains that can be transformed into all-atom models without atom clashes. To this end, an iterative trial-and-error procedure was used. Rigid WLR models of cruciate units were fixed in space at certain distances and joined by flexible WLR fragments [54] of necessary lengths. The harmonic parameters of the WLR model were earlier chosen so that in Monte Carlo and Brownian dynamics simulations the chains were statistically close to B-DNA, namely, the average twist  $33.5^\circ$ , the average rise  $3.3 \text{ \AA}$ , the bending persistence length  $50 \text{ nm}$ , and the torsional persistence length  $90 \text{ nm}$ . These fragments were kept at distances of about  $25 \text{ \AA}$  by harmonic restraints and the system was rapidly relaxed by short MD followed by energy minimization. After that the helical parameters of the flexible fragments were checked. The twist and rise values almost did not vary along the flexible chains and the distances between the cruciate units were changed by trials to push the corresponding values to the harmonic minima. The final WLR models were back-transformed into all atom structures. With the helical parameters close to B-DNA and the absence of strong bends, the backbone junctions were easily corrected by vacuum energy minimization, with position restraints applied to bases only.

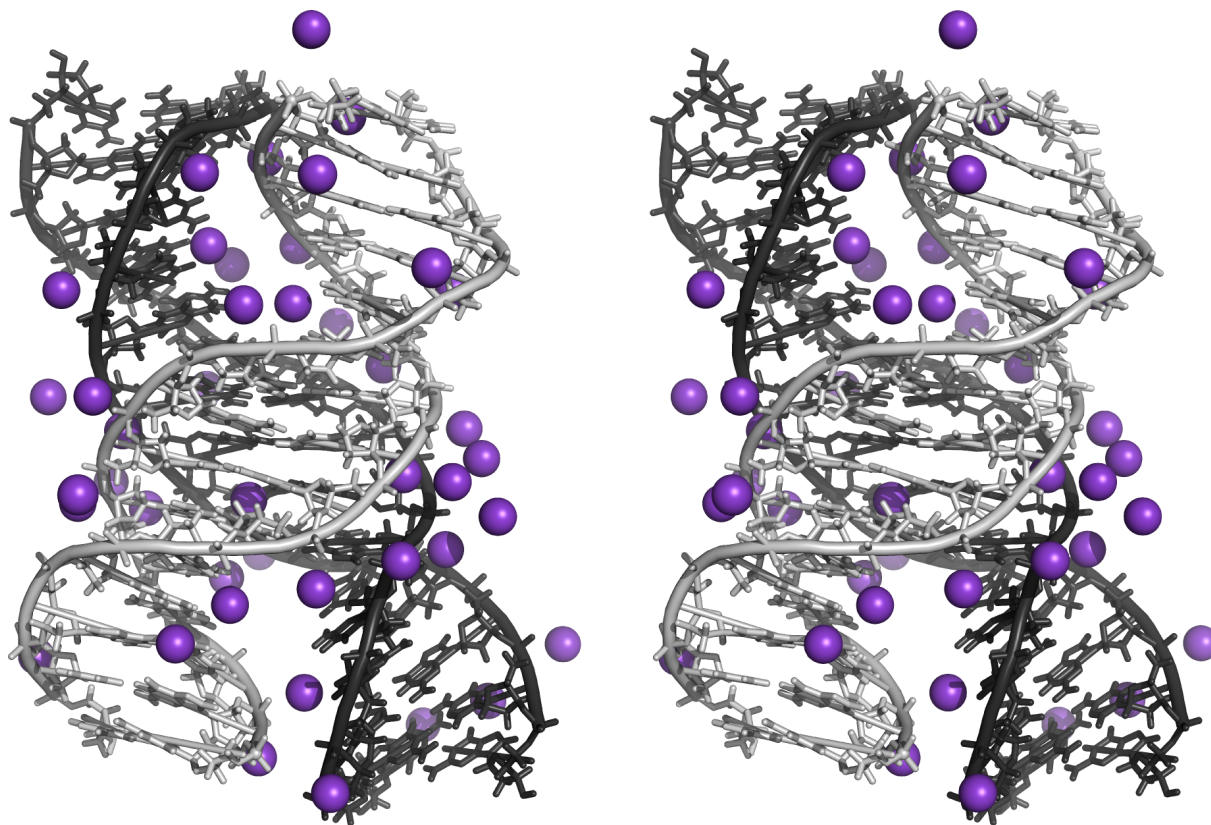


FIG. S2: A snapshot from the dissociation pathway with the cruciate structure used for modeling complexes of long DNA presented in Fig. 5. The solvent is not included except for potassium ions from the 10 Å vicinity of the complex. A cross-eyed stereo image is shown.

#### Trajectory animation files

Files fold1.mp4 and fold2.mp4 show two perpendicular views of the consecutive states from the trajectory starting from the predicted intermediate state and continued to the bound state (folding). The movies represent cross-eyed stereograms of DNA with potassium ions from the

10 Å vicinity of backbone atoms. Water molecules are not shown. Files unfold1.mp4 and unfold2.mp4 present similar data from the trajectory starting from the same intermediate state and continued to dissociation (unfolding). The animation files were prepared with PyMOL program.